Prion 3:3, 139-145; July/August/Septmeber, 2009; © 2009 Landes Bioscience

Towards revealing the structure of bacterial inclusion bodies

Lei Wang

Laboratory of Physical Chemistry; Swiss Federal Institute of Technology (ETH); Zurich, Switzerland

Key words: bacterial, inclusion bodies, amyloid fibrils, protein aggregation, amyloid-like, nuclear magnetic resonance, electron microscope, X-ray diffraction, hydrogen/deuterium exchange, cross-β

Abbreviations: EM, electron microscope; NMR, nuclear magnetic resonance; H/D-exchange, hydrogen/deuterium exchange; FTIR, fourier transform infrared red spectroscopy; ESAT-6, early secreted antigen 6-kDa protein; BMP2(13-74), residues 13-74 of the secretory human bone morphogenetic protein-2

Protein aggregation is a widely observed phenomenon in human diseases, biopharmaceutical production, and biological research. Protein aggregates are generally classified as highly ordered, such as amyloid fibrils, or amorphous, such as bacterial inclusion bodies. Amyloid fibrils are elongated filaments with diameters of 6–12 nm, they are comprised of residue-specific cross-β structure, and display characteristic properties, such as binding with amyloid-specific dyes. Amyloid fibrils are associated with dozens of human pathological conditions, including Alzheimer disease and prion diseases. Distinguished from amyloid fibrils, bacterial inclusion bodies display apparent amorphous morphology. Inclusion bodies are formed during high-level recombinant protein production, and formation of inclusion bodies is a major concern in biotechnology. Despite of the distinctive morphological difference, bacterial inclusion bodies have been found to have some amyloid-like properties, suggesting that they might contain structures similar to amyloid-like fibrils. Recent structural data further support this hypothesis, and this review summarizes the latest progress towards revealing the structural details of bacterial inclusion bodies.

Introduction

Protein aggregation is a widely observed phenomenon in human diseases, biopharmaceutical production and biological research. Based on their morphology, protein aggregates are generally classified as either highly ordered, as in the case of amyloid fibrils, or amorphous, as in the case of bacterial inclusion bodies.

The term "amyloid" was first introduced by Rudolf Virchow to describe the starch-like pale waxy tissue abnormality,[1] and amyloid fibrils are associated with dozens of human pathological conditions, including Alzheimer disease, Parkinson disease, diabetes type II and prion diseases.[2-5] It has also been reported that a variety of bacteria can make functional amyloids.[6-10] Under the electron microscope (EM), amyloid fibrils are elongated filaments with diameters of 6–12 nm.[11-13] X-ray diffraction of aligned amyloid fibrils shows a characteristic pattern with a meridional reflection at 4.7 Å and an equatorial reflection at ~10 Å, indicating a cross-β structure.[14,15] High-resolution structural studies have shown that these filaments are comprised of sequence-specific cross-β structure, with intermolecular and in-register β-sheets parallel to the filament axis.[15-24] Amyloid fibrils can bind with amyloid-specific dyes, such as Congo red[25,26] and thioflavin T,[27] and can be infectious and toxic as represented by the HET-s prion system.[18,28]

Distinguished from amyloid fibrils, bacterial inclusion bodies are classified as amorphous aggregates. They are protein aggregates generated during recombinant protein production in bacteria, and are a major concern in biotechnology.[29,30] Formation of inclusion bodies may be caused by the high local concentration of nascent polypeptides emerging from ribosomes during overexpression, and insufficient chaperones presenting around to protect these nascent polypeptides from aggregation.[29,31-33] Bacterial inclusion bodies are not just unstructured aggregates that are clusters of misfolded proteins sticking to each other through non-specific hydrophobic interactions.[34,35] Rather, studies have shown that inclusion bodies have amyloid-like properties,[30,32,36-43] i.e., binding with Congo red and showing birefringence (**Fig. 1**), seeding the aggregation of their soluble counterpart[39] and inducing cytotoxicity in eukaryotic cells.[44] These properties are indicative that inclusion bodies might contain structure reminiscent of amyloid fibrils. Indeed, recent data that further support this hypothesis have been presented, and it is the aim of this review to summarize the current progress towards revealing the structure of bacterial inclusion bodies.

Morphology of Inclusion Bodies

When inclusion bodies are formed, they are normally observed under EM as large, dark aggregates inside the host cells[45-47] (**Fig. 2A**). After purified from cell lysate, inclusion bodies are amorphous (**Fig. 2B**), approximating sphere-like or rod-like shapes with diameters ranging from 0.2 μm to 1.2 μm.[39,48-52] The size of inclusion bodies is probably related to the dimensions of the host cells in which they were produced, the protein sequences,

*Correspondence to: Lei Wang; Email: leiwang@phys.chem.ethz.ch
Submitted: 04/02/09; Accepted: 08/25/09
Previously published online:
www.landesbioscience.com/journals/prion/article/9922

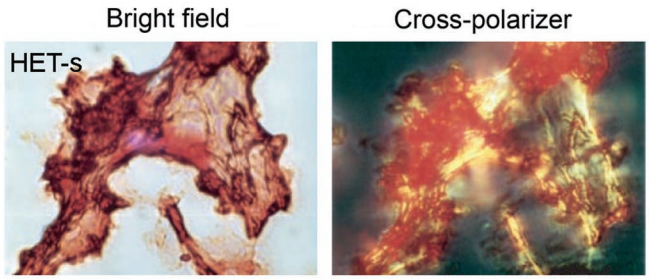

Figure 1. Congo red binding with amyloid fibrils and bacterial inclusion bodies. Congo red staining under bright field (left) and showing birefringence under cross-polarized light (right) when binding with amyloid fibrils of HET-s (upper) and inclusion bodies of mouse prion protein PrP(23-231) (lower). (Partial reproduction of Figs. 2,[26] and S8,[52]).

and the physical conditions during protein production. Inclusion bodies of some proteins also release amyloid-like protofibrils or fibrils under certain conditions, examples are: (1) BMP2(13-74) incubated at 37°C for 12 hours[52] (**Fig. 2C**); (2) BMP2(13-74) produced in host cells for 12 hours[52] (**Fig. 2D**); (3) BMP2(13-74) partially disaggregated by 4 M urea solution (**Fig. 2E**); (4) ESAT-6 incubated at room temperature for 14 days[52] (**Fig. 2F**); (5) Aβ42-GFP and Aβ42 after proteinase K proteolytic action[53] (**Fig. 2G**); (6) HET-s(218-289) after three hours of expression[46] (**Fig. 2H**). Since inclusion bodies of BMP2(13-74) and ESAT-6 do not display fibrils right after three hours of expression, it is possible that these inclusion bodies mainly contain immature and flexible protofibrils that mature into fibrils given time and proper temperature. On the other hand, the inclusion bodies of highly aggregation-prone, prion-forming domain, HET-s(218-289), may contain mature fibrils.

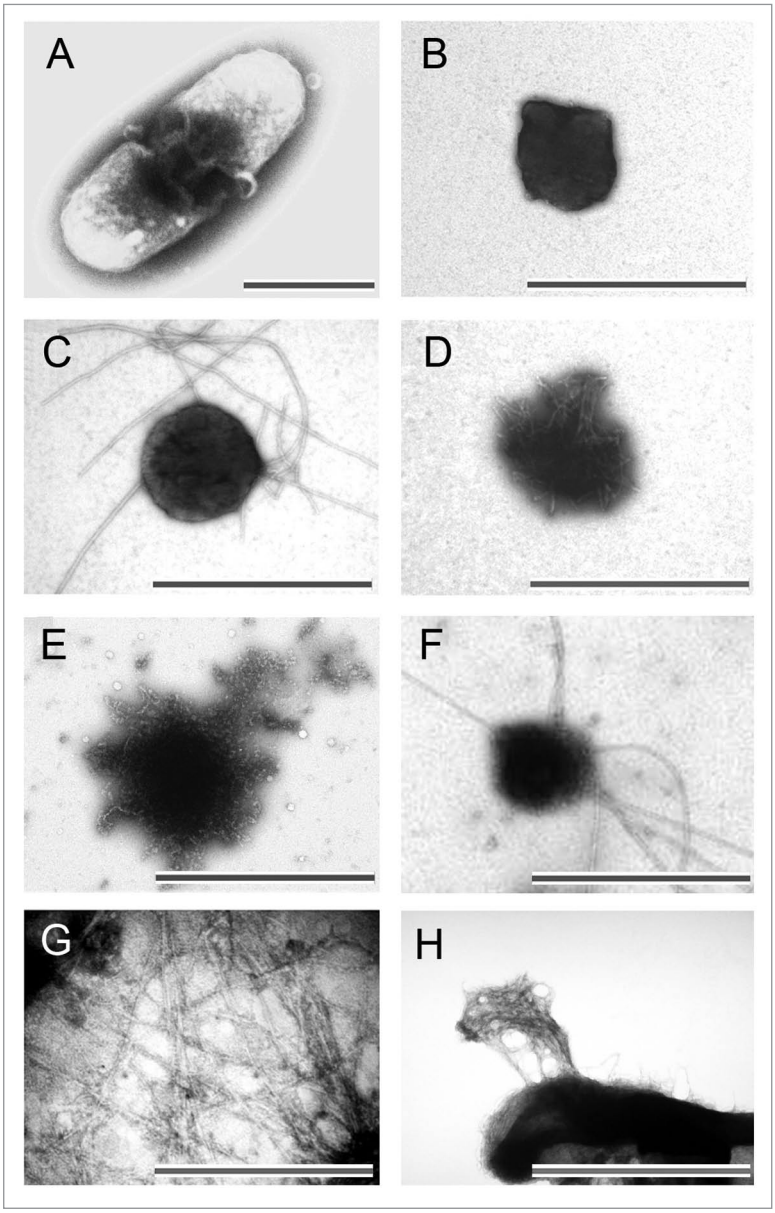

Inclusion Bodies are Often Enriched in β-Sheet Secondary Structure

The apparent amorphous inclusion bodies of different proteins were examined by Fourier transform infrared red (FTIR) spectroscopy, which is a method to analyze the secondary structure content of proteins in soluble as well as in aggregated form. For the FTIR spectrum of soluble VP1LAC, a β-galactosidase derivative with N-terminally fused VP1 capsid protein, peaks at ~1,634 cm^{-1}, ~1,644 cm^{-1} and ~1,654 cm^{-1} are usually assigned to the β-sheet, random coil and α-helix conformations of the protein, respectively[39] (**Fig. 3A**). In the FTIR spectrum of inclusion bodies of VP1LAC, additional sharp peaks at ~1,621 cm^{-1} and ~1,691 cm^{-1} emerge compared to the spectrum of soluble protein (**Fig. 3A**), which are indicative of newly formed β-sheet structures in inclusion bodies.[39,53-57] For some proteins, the FTIR spectra of their inclusion bodies also show peaks at ~1,634 cm^{-1} and ~1,651 cm^{-1} (**Fig. 3A**), which suggests

Figure 2. Morphology of bacterial inclusion bodies observed under electron microscope. (A) An *E. coli* cell containing inclusion body of ESAT-6, (B) Inclusion bodies of BMP2(13-74) after purification, (C) Inclusion body of BMP2(13-74) after incubation at 37°C for 12 hours, (D) Inclusion body of BMP2(13-74) after grown in host cells for 12 hours, (E) Inclusion body of BMP2(13-74) after disaggregated in 4 M of urea solution, (F) Inclusion body of ESAT-6 after incubation at room temperature for 14 days, (G) Inclusion body of Aβ42 after proteinase K proteolytic action, (H) Inclusion body of HET-s(218-289) after three hours expression. Scale bars indicate 1 μm. (Partial reproduction of Figs. 5, S7,[52] 5,[53] and S4,[46]).

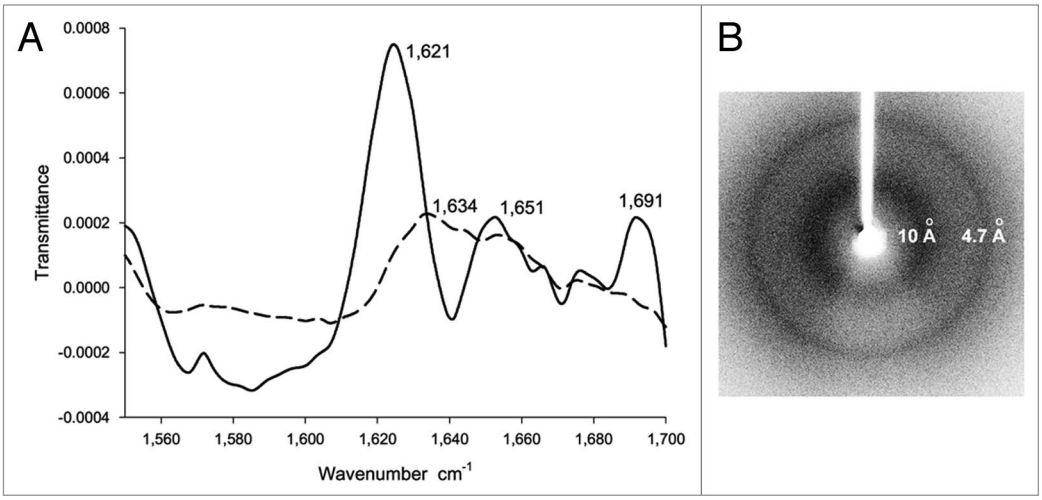

Figure 3. (A) The FTIR spectrum of inclusion bodies of VP1LAC (continuous line) and soluble VP1LAC (broken line). VP1LAC stays in the soluble cell fraction as well as in inclusion bodies when produced in *E. coli*. (B) The X-ray diffraction of inclusion bodies of ESAT-6. (Partial reproduction of Figs. 8,[39] and 2,[52]).

that these inclusion bodies also contain residual native-like β-sheet and α-helix structures of their soluble form.[39,54-62]

Inclusion Bodies Contain Cross-β Structure

Although no 3D structure of inclusion bodies is available, the tertiary structural content of inclusion bodies is, at least partially, determined by X-ray diffraction.[52,63] The X-ray diffraction spectra of inclusion bodies shows a two-ring diffraction pattern (**Fig. 3B**), typical for the cross-β structure in amyloid fibrils, with a major reflection at 4.7 Å resolution interpreted as the spacing between strands in a β-sheet and a diffused reflection at ~10 Å interpreted as the spacing between β-sheets. The circular profiles of the two reflections, rather than the typical orthogonal positions for the cross-β structure in amyloid fibrils, show that the cross-β structural entities in inclusion bodies are not strongly aligned as in amyloid fibrils.

The Cross-β Structure of Inclusion Bodies is Residue-Specific and Amyloid-Like

(a) Structural studies of inclusion bodies of ESAT-6, BMP2 (13-74) and MOG(ECD).[52] To elucidate the residue-specific structural information, quenched hydrogen/deuterium exchange (H/D-exchange) experiments with solution nuclear magnetic resonance (NMR) were measured for three inclusion body-forming proteins that have distinctive native soluble folds that cover the folding spectrum: (1) The α-helical early secreted antigen 6-kDa protein (ESAT-6) (ESAT-6 folds only in complex with its protein partner CFP-10);[64] (2) The mixed α-helical and β-sheet protein, residues 13-74 of the secretory human bone morphogenetic protein-2 [BMP2(13-74)];[65,66] (3) The β-sheet extracellular domain of the human membrane protein myelin oligodendrocyte glycoprotein [MOG (ECD)] [MOG(ECD) contains one disulfide bridge].[67,68] Inclusion bodies of all three proteins bind Congo red and thioflavin T, suggesting that they contain amyloid-like structures.

In the case of ESAT-6 inclusion bodies, residues 7-23 form hydrogen bonds as identified by NMR H/D-exchange experiment (**Fig. 4**). **Figure 4A** (left) is the [^{15}N,^{1}H]-correlation NMR spectrum of dissolved monomeric ESAT-6 inclusion bodies, which contains cross-peaks corresponding to its backbone amides. Upon exchange of the inclusion bodies in D_2O buffer for 311 hours, only cross-peaks of residues 8-25 and 36-43 are still present (**Fig. 4A**, right), which is indicative of slow exchange. The H/D-exchange was followed over time, and it was found that all residues in the inclusion bodies display a heterogeneous biphasic behavior, with a very fast and a slow exchanging component (**Fig. 4C**). The detailed analysis of the H/D-exchange data shows that the major population (**Fig. 4D** and $p > 1/2$) of residues 7-23 in ESAT-6 inclusion bodies display slow exchange rates of 10^{-3} to 10^{-4} h^{-1} and are therefore considered to be involved in hydrogen bonds (**Fig. 4B** and **D**). In contrast, the majority of residues 2-6 and 24-95 (**Fig. 4D** and $p > 1/2$) display fast exchange rates larger than 10^{1} h^{-1} and are therefore considered to be unprotected in H/D-exchange and conformationally disordered. Because soluble ESAT-6 is a α-helical protein, but the circular dichroism spectrum of ESAT-6 inclusion bodies is indicative of β-sheet conformation, and the x-ray diffraction shows a two-ring pattern that is typical for a cross-β structure,[52] it is likely that the hydrogen bond-forming residues 7-23 of ESAT-6 contain a mainly amyloid-like, cross-β structure in its inclusion bodies.

To verify that residues 7-23 comprise the dominant component in the formation of cross-β structure in ESAT-6 inclusion bodies, aggregation-prone residues in ESAT-6 were mutated to the aggregation-interfering residue Arg.[69] It was found that only the mutations F8R, I11R, I18R or V22R within the residue 7-23 segment abolished the formation of inclusion bodies, but not the mutations L36R, V54R or I76R. To confirm that residues 7-23 can form an amyloid-like cross-β structure, a peptide E20 corresponding to residues 6-25 of ESAT-6 was synthesized, and it can form amyloid fibrils under physiological conditions. In summary, residues 7-23 of ESAT-6 in bacterial inclusion bodies form

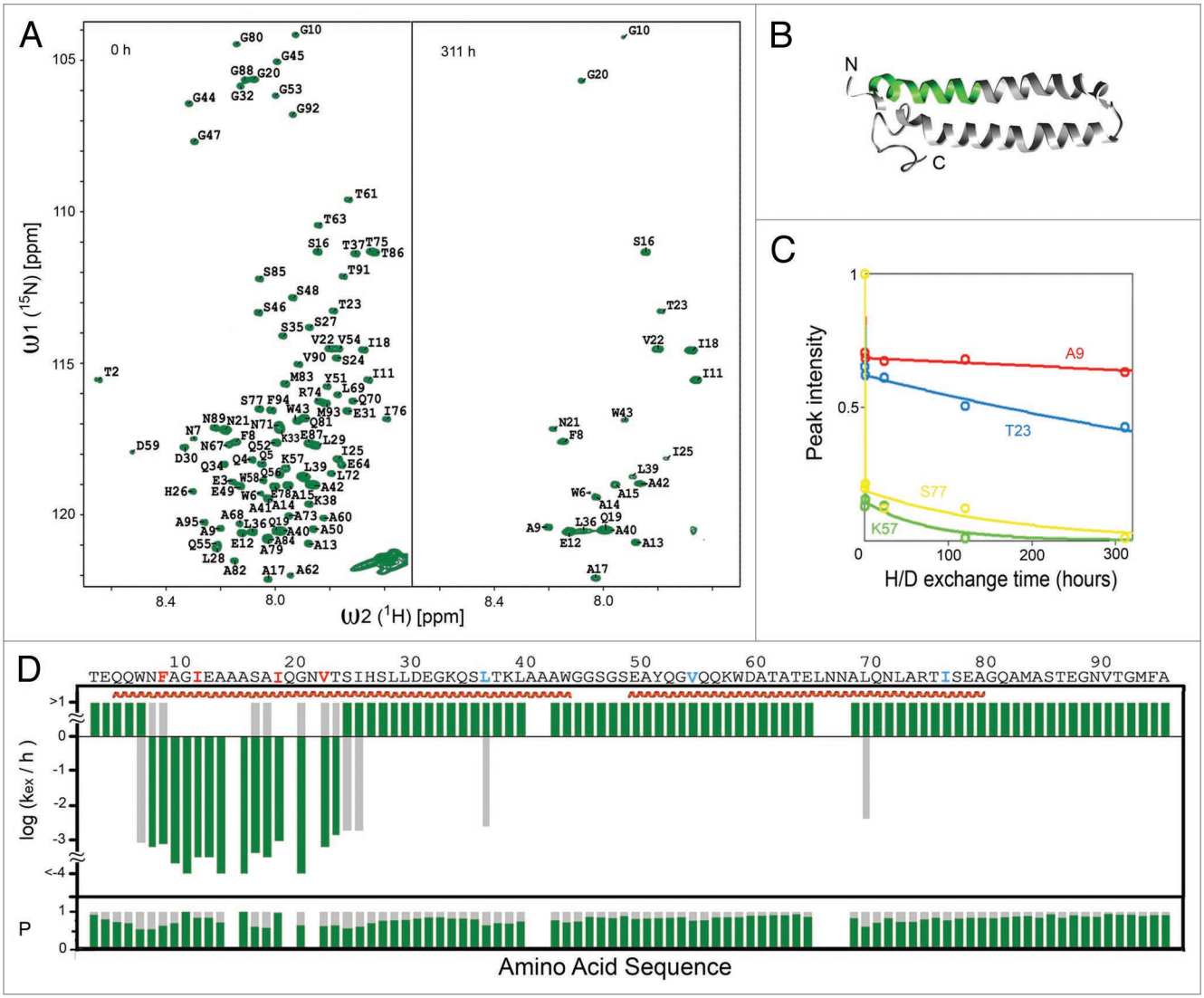

Figure 4. Residues 7-23 of ESAT-6 form cross-β structure in inclusion bodies (A) [^{15}N,^{1}H]-HMQC-spectra of dissolved monomeric ESAT-6 inclusion bodies before (left) and after (right) exchanged in D_2O buffer for 311 hours. (B) Ribbon representation of the 3D structure of soluble ESAT-6, while in complex with CFP-10 (not shown).[64] The green-colored segment corresponds to residues 7-23. (C) NMR H/D-exchange curves for residues A9, T23, K57 and S77 of ESAT-6. The peak intensities for each residue were plotted versus the H/D exchange time. (D) H/D-exchange rates k_{ex}/h, and the relative population P of the two exchange components against the amino acid sequence of ESAT-6. The exchange rates of the major population (p > 1/2) are colored green. If the minor population (p < 1/2) is present more than 1/3, the corresponding exchange rates are shown in grey. The secondary structures of the soluble conformation shown in (B) are highlighted in red. (Partial reproduction of Figs. 2 and S2,[52]).

a cross-β structure characteristic of amyloid-like fibrils with the remainder of sequence disordered.

In the case of BMP2(13-74) and MOG(ECD), similar results were also found: residues 62-67 of BMP2(13-74) and residues 85-95, 101-108, 111-118 of MOG(ECD) form a cross-β structure characteristic of amyloid-like fibrils with the remainder of the amino acid sequence disordered.

(b) **Structural study of inclusion bodies of HET-s(218-289).**[46] [Het-s] is a prion protein involved in the self-recognition of the filamentous fungus *P. anserina*.[70] The C-terminal region containing residues 218-289 of [Het-s] [HET-s(218-289)] is the prion-forming domain.[18,71] HET-s(218-289) can form amyloid fibrils, which contain a β-solenoid with two layers of β-strands per monomer and is characterized by the formation of a triangular hydrophobic core.[22] During protein production, HET-s(218-289) forms inclusion bodies that display [Het-s] prion infectivity.[46] The ^{13}C-^{13}C proton-driven spin-diffusion (PDSD) spectra with solid-state NMR was measured for the inclusion bodies of HET-s(218-289), and the spectra reproduces all the cross-peaks visible for the amyloid fibrils of HET-s(218-289) (**Fig. 5**). Since the NMR chemical shifts are strongly dependent on the conformation of a polypeptide, the same chemical shifts of inclusion bodies and amyloid fibrils of HET-s(218-289) suggest that their molecular structures have to be virtually the same. This conclusion is also supported by NMR H/D-exchange data, which shows that the exchange pattern of the purified inclusion

bodies closely resembles the exchange pattern of the HET-s(218-289) fibrils.

Heterogeneity of Inclusion Bodies

In addition to amyloid-like structure, native-like structure could be retained in inclusion bodies of some proteins,[39,54-62,72] and inclusion bodies may contain phospholipids from the *E. coli* membrane as well as other proteins and possibly RNA.[46] Also the H/D-exchange of solution NMR shows that a small population (usually less than 1/3) of protein inside inclusion bodies have different exchange rates than the major population that forms amyloid-like structure,[52] indicating structural heterogeneity in inclusion bodies. So it is possible that, besides contaminants, inclusion bodies are comprised of mixtures of amyloid-like protofibrils/fibrils with unfolded, partially folded or even natively folded proteins.[73] The ratio of amyloid-like structure versus other heterogeneous structure could be affected by several factors, such as the stability of the protein in its native fold, or the physical parameters used during protein production.[54]

The structural study of inclusion bodies of FHA2 provides a residue-specific analysis to show that inclusion bodies retain at least part of their native-like structure.[72] FHA2 is the N-terminal 185-residue functional domain of the 221-residue HA2 subunit of the influenza virus hemagglutinin protein.[74] Its sequence contains several "sequential pairs." By selectively [^{13}C,^{15}N]-labeling these "sequential pairs" and measuring the rotational-echo double-resonance (REDOR) with solid-state NMR[75] for the inclusion bodies of FHA2, REDOR can detect the signal of ^{13}C carbonyl (^{13}CO) nuclei which are directly bonded to ^{15}N nuclei in the protein sequence. By comparing the backbone ^{13}CO chemical shifts of these residues to the chemical shift of α-helix and β-sheet, the local secondary structure of FHA2 inclusion bodies can be determined. It was found that the backbone ^{13}CO chemical shifts of residues Gly-1, Gly-4, Ala-7 and Leu-98 of FHA2 in inclusion bodies indicate an α-helix conformation. Considering that in the native soluble fold of FHA2, residues Gly-1, Gly-4 and Ala-7 lie in a N-terminal α-helix, and Leu-98 lies in an α-helix spanning residues 38-105, it suggests that some native-like structure is retained in inclusion bodies of FHA2.

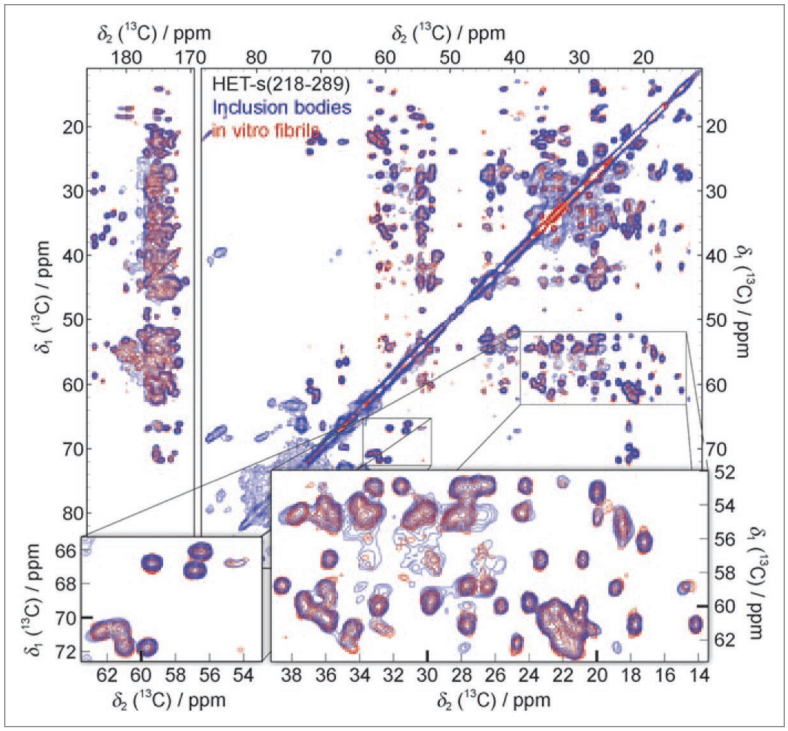

Figure 5. ^{13}C-^{13}C solid-state NMR correlation spectrum of purified HET-s(218-289) inclusion bodies (blue) compared to a spectrum of in vitro fibrillized HET-s(218-289) (red). Additional cross-peaks, not belonging to HET-s(218-289), at ~34 ppm, ~60–100 ppm and ~176–180 ppm are assigned to phospholipids, other proteins and RNA from *E. coli*. (Reproduction of Fig. 3,[46]).

Summary

Current structural studies have revealed that beneath the amorphous appearance, bacterial inclusion bodies are actually structured aggregates that contain residue-specific cross-β structure reminiscent of amyloid-like protofibrils or fibrils. Inclusion bodies may also contain a portion of heterogeneously structured proteins that may be native-like, partially folded or unstructured, and could retain native-like biological activities.[76-79] High-resolution 3D structures of inclusion bodies need to be solved to understand their architecture in depth. Structural comparison of inclusion bodies and amyloid fibrils of HET-s(218-289) suggests that they share the same structure, and it would be interesting to make this comparison on proteins that are less aggregation-prone. Since polymorphism plays an important role in the formation of amyloid fibrils,[80,81] it might also induce different cross-β structure in inclusion bodies and amyloid fibrils of the same protein.

By assuming that the observed amyloid-like nature of inclusion bodies holds for most of the other documented bacterial inclusion bodies,[82] amyloid-like aggregation is probably a common intrinsic property of protein segments and consequently is observed in both eukaryotes and prokaryotes.[3] These structural studies of bacterial inclusion bodies thus extend the possible structural landscape of proteins: in addition to an unfolded or folded state, each protein may also contain one or more segments that are capable of forming a sequence-specific, cross-β-sheet aggregated state. "The process of protein aggregation can thus be viewed as a primitive folding mechanism, resulting in a defined aggregated conformation with each aggregated protein having its own distinctive properties."[52]

Acknowledgements

I want to thank Prof. Roland Riek, Dr. Christos Tzitzilonis, Dr. Jason Greenwald and Carolin Buhtz for providing valuable comments and suggestions for this review.

References

1. Sipe JD, Cohen AS. Review: history of the amyloid fibril. J Struct Biol 2000; 130:88-98.
2. Selkoe DJ. Folding proteins in fatal ways. Nature 2003; 426:900-4.
3. Dobson CM. Protein folding and misfolding. Nature 2003; 426:884-90.
4. Kelly JW. Attacking amyloid. N Engl J Med 2005; 352:722-3.
5. Tanaka M, Collins SR, Toyama BH, Weissman JS. The physical basis of how prion conformations determine strain phenotypes. Nature 2006; 442:585-9.
6. Alteri CJ, Xicohtencatl-Cortes J, Hess S, Caballero-Olin G, Giron JA, Friedman RL. *Mycobacterium tuberculosis* produces pili during human infection. Proc Natl Acad Sci USA 2007; 104:5145-50.
7. Chapman MR, Robinson LS, Pinkner JS, Roth R, Heuser J, Hammar M, et al. Role of *Escherichia coli* curli operons in directing amyloid fiber formation. Science 2002; 295:851-5.
8. Jordal PB, Dueholm MS, Larsen P, Petersen SV, Enghild JJ, Christiansen G, et al. Widespread abundance of functional bacterial amyloid in mycolata and other gram-positive bacteria. Appl Environ Microbiol 2009; 75:4101-10.
9. Claessen D, Rink R, de Jong W, Siebring J, de Vreugd P, Boersma FG, et al. A novel class of secreted hydrophobic proteins is involved in aerial hyphae formation in Streptomyces coelicolor by forming amyloid-like fibrils. Genes Dev 2003; 17:1714-26.
10. Oh J, Kim JG, Jeon E, Yoo CH, Moon JS, Rhee S, Hwang I. Amyloidogenesis of type III-dependent harpins from plant pathogenic bacteria. J Biol Chem 2007; 282:13601-9.
11. Maji SK, Perrin MH, Sawaya MR, Jessberger S, Vadodaria K, Rissman RA, et al. Functional Amyloids as Natural Storage of Peptide Hormones in Pituitary Secretory Granules. Science 2009; 325:328-32..
12. Maji SK, Schubert D, Rivier C, Lee S, Rivier JE, Riek R. Amyloid as a depot for the formulation of long-acting drugs. PLoS Biol 2008; 6:17.
13. Siemer AB, Ritter C, Steinmetz MO, Ernst M, Riek R, Meier BH. ^{13}C, ^{15}N resonance assignment of parts of the HET-s prion protein in its amyloid form. J Biomol NMR 2006; 34:75-87.
14. Astbury WT, Dickinson S. The X-ray interpretation of denaturation and the structure of the seed globulins. Biochem J 1935; 29:2351-60.
15. Sunde M, Serpell LC, Bartlam M, Fraser PE, Pepys MB, Blake CC. Common core structure of amyloid fibrils by synchrotron X-ray diffraction. J Mol Biol 1997; 273:729-39.
16. Kirschner DA, Abraham C, Selkoe DJ. X-ray diffraction from intraneuronal paired helical filaments and extraneuronal amyloid fibers in Alzheimer disease indicates cross-beta conformation. Proc Natl Acad Sci USA 1986; 83:503-7.
17. Nelson R, Sawaya MR, Balbirnie M, Madsen AO, Riekel C, Grothe R, Eisenberg D. Structure of the cross-beta spine of amyloid-like fibrils. Nature 2005; 435:773-8.
18. Ritter C, Maddelein ML, Siemer AB, Luhrs T, Ernst M, Meier BH, et al. Correlation of structural elements and infectivity of the HET-s prion. Nature 2005; 435:844-8.
19. Luhrs T, Ritter C, Adrian M, Riek-Loher D, Bohrmann B, Dobeli H, et al. 3D structure of Alzheimer's amyloid-beta(1-42) fibrils. Proc Natl Acad Sci USA 2005; 102:17342-7.
20. Sawaya MR, Sambashivan S, Nelson R, Ivanova MI, Sievers SA, Apostol MI, et al. Atomic structures of amyloid cross-beta spines reveal varied steric zippers. Nature 2007; 447:453-7.
21. Petkova AT, Ishii Y, Balbach JJ, Antzutkin ON, Leapman RD, Delaglio F, Tycko R. A structural model for Alzheimer's beta-amyloid fibrils based on experimental constraints from solid state NMR. Proc Natl Acad Sci USA 2002; 99:16742-7.
22. Wasmer C, Lange A, Van Melckebeke H, Siemer AB, Riek R, Meier BH. Amyloid fibrils of the HET-s(218-289) prion form a beta solenoid with a triangular hydrophobic core. Science 2008; 319:1523-6.
23. Maji SK, Wang L, Greenwald J, Riek R. Structure-Activity Relationship of Amyloid Fibrils. FEBS Lett 2009.
24. Vilar M, Chou HT, Luhrs T, Maji SK, Riek-Loher D, Verel R, et al. The fold of alpha-synuclein fibrils. Proc Natl Acad Sci USA 2008; 105:8637-42.
25. Westermark GT, Johnson KH, Westermark P. Staining methods for identification of amyloid in tissue. Methods in Enzymology 1999; 309:3-25.
26. Dos Reis S, Coulary-Salin B, Forge V, Lascu I, Begueret J, Saupe SJ. The HET-s prion protein of the filamentous fungus *Podospora anserina* aggregates in vitro into amyloid-like fibrils. J Biol Chem 2002; 277:5703-6.
27. LeVine H, 3rd. Quantification of beta-sheet amyloid fibril structures with thioflavin T. Methods Enzymol 1999; 309:274-84.
28. Maddelein ML, Dos Reis S, Duvezin-Caubet S, Coulary-Salin B, Saupe SJ. Amyloid aggregates of the HET-s prion protein are infectious. Proc Natl Acad Sci USA 2002; 99:7402-7.
29. Ventura S. Sequence determinants of protein aggregation: tools to increase protein solubility. Microb Cell Fact 2005; 4:11.
30. Ventura S, Villaverde A. Protein quality in bacterial inclusion bodies. Trends Biotechnol 2006; 24:179-85.
31. Freedman RB, Wetzel R. Protein engineering. Curr Opin Biotechnol 1992; 3:323-5.
32. Chrunyk BA, Evans J, Lillquist J, Young P, Wetzel R. Inclusion body formation and protein stability in sequence variants of interleukin-1beta. J Biol Chem 1993; 268:18053-61.
33. Rinas U, Bailey JE. Protein compositional analysis of inclusion bodies produced in recombinant *Escherichia coli*. Appl Microbiol Biotechnol 1992; 37:609-14.
34. Rousseau F, Schymkowitz J, Serrano L. Protein aggregation and amyloidosis: confusion of the kinds? Curr Opin Struct Biol 2006; 16:118-26.
35. Fink AL. Protein aggregation: folding aggregates, inclusion bodies and amyloid. Fold Des 1998; 3:9-23.
36. de Groot NS, Sabate R, Ventura S. Amyloids in bacterial inclusion bodies. Trends Biochem Sci 2009; 34:408-16.
37. Speed MA, Wang DI, King J. Specific aggregation of partially folded polypeptide chains: the molecular basis of inclusion body composition. Nat Biotechnol 1996; 14:1283-7.
38. King J, Haase-Pettingell C, Robinson AS, Speed M, Mitraki A. Thermolabile folding intermediates: inclusion body precursors and chaperonin substrates. Faseb J 1996; 10:57-66.
39. Carrio M, Gonzalez-Montalban N, Vera A, Villaverde A, Ventura S. Amyloid-like properties of bacterial inclusion bodies. J Mol Biol 2005; 347:1025-37.
40. Wang X, Fu M, Ren J, Qu X. Evaluation of different culture conditions for high-level soluble expression of human cyclin A2 with pET vector in BL21 (DE3) and spectroscopic characterization of its inclusion body structure. Protein Expr Purif 2007; 56:27-34.
41. de Groot NS, Espargaro A, Morell M, Ventura S. Studies on bacterial inclusion bodies. Future Microbiol 2008; 3:423-35.
42. Carrio MM, Corchero JL, Villaverde A. Dynamics of in vivo protein aggregation: building inclusion bodies in recombinant bacteria. FEMS Microbiol Lett 1998; 169:9-15.
43. Carrio MM, Villaverde A. Role of molecular chaperones in inclusion body formation. FEBS Lett 2003; 537:215-21.
44. Gonzalez-Montalban N, Villaverde A, Aris A. Amyloid-linked cellular toxicity triggered by bacterial inclusion bodies. Biochem Biophys Res Commun 2007; 355:637-42.
45. Betton JM, Hofnung M. Folding of a mutant maltose-binding protein of *Escherichia coli* which forms inclusion bodies. J Biol Chem 1996; 271:8046-52.
46. Wasmer C, Benkemoun L, Sabate R, Steinmetz MO, Coulary-Salin B, Wang L, et al. Solid-state NMR spectroscopy reveals that *E. coli* inclusion bodies of HET-s(218-289) are amyloids. Angew Chem Int Ed Engl 2009; 48:4858-60.
47. Zhu C, Yu Z. The surface layer protein of *Bacillus thuringiensis* CTC forms unique intracellular parasporal inclusion body. J Basic Microbiol 2008; 48:302-7.
48. Carrio MM, Cubarsi R, Villaverde A. Fine architecture of bacterial inclusion bodies. FEBS Lett 2000; 471:7-11.
49. Kang H, Sun AY, Shen YL, Wei DZ. Refolding and structural characteristic of TRAIL/Apo2L inclusion bodies from different specific growth rates of recombinant *Escherichia coli*. Biotechnol Prog 2007; 23:286-92.
50. Singh SM, Panda AK. Solubilization and refolding of bacterial inclusion body proteins. J Biosci Bioeng 2005; 99:303-10.
51. Bowden GA, Paredes AM, Georgiou G. Structure and morphology of protein inclusion bodies in *Escherichia coli*. Biotechnology (NY) 1991; 9:725-30.
52. Wang L, Maji SK, Sawaya MR, Eisenberg D, Riek R. Bacterial inclusion bodies contain amyloid-like structure. PLoS Biol 2008; 6:195.
53. Morell M, Bravo R, Espargaro A, Sisquella X, Aviles FX, Fernandez-Busquets X, Ventura S. Inclusion bodies: specificity in their aggregation process and amyloid-like structure. Biochim Biophys Acta 2008; 1783:1815-25.
54. Ami D, Natalello A, Gatti-Lafranconi P, Lotti M, Doglia SM. Kinetics of inclusion body formation studied in intact cells by FT-IR spectroscopy. FEBS Lett 2005; 579:3433-6.
55. Ami D, Natalello A, Taylor G, Tonon G, Maria Doglia S. Structural analysis of protein inclusion bodies by Fourier transform infrared microspectroscopy. Biochim Biophys Acta 2006; 1764:793-9.
56. Umetsu M, Tsumoto K, Ashish K, Nitta S, Tanaka Y, Adschiri T, Kumagai I. Structural characteristics and refolding of in vivo aggregated hyperthermophilic archaeon proteins. FEBS Lett 2004; 557:49-56.
57. Gonzalez-Montalban N, Garcia-Fruitos E, Ventura S, Aris A, Villaverde A. The chaperone DnaK controls the fractioning of functional protein between soluble and insoluble cell fractions in inclusion body-forming cells. Microb Cell Fact 2006; 5:26.
58. Przybycien TM, Dunn JP, Valax P, Georgiou G. Secondary structure characterization of beta-lactamase inclusion bodies. Protein Eng 1994; 7:131-6.
59. Umetsu M, Tsumoto K, Nitta S, Adschiri T, Ejima D, Arakawa T, Kumagai I. Nondenaturing solubilization of beta2 microglobulin from inclusion bodies by L-arginine. Biochem Biophys Res Commun 2005; 328:189-97.
60. Doglia SM, Ami D, Natalello A, Gatti-Lafranconi P, Lotti M. Fourier transform infrared spectroscopy analysis of the conformational quality of recombinant proteins within inclusion bodies. Biotechnol J 2008; 3:193-201.
61. Oberg K, Chrunyk BA, Wetzel R, Fink AL. Nativelike secondary structure in interleukin-1beta inclusion bodies by attenuated total reflectance FTIR. Biochemistry 1994; 33:2628-34.
62. Jevsevar S, Gaberc-Porekar V, Fonda I, Podobnik B, Grdadolnik J, Menart V. Production of nonclassical inclusion bodies from which correctly folded protein can be extracted. Biotechnol Prog 2005; 21:632-9.

63. Ignatova Z, Gierasch LM. Aggregation of a slow-folding mutant of a beta-clam protein proceeds through a monomeric nucleus. Biochemistry 2005; 44:7266-74.
64. Renshaw PS, Lightbody KL, Veverka V, Muskett FW, Kelly G, Frenkiel TA, et al. Structure and function of the complex formed by the tuberculosis virulence factors CFP-10 and ESAT-6. EMBO J 2005; 24:2491-8.
65. Scheufler C, Sebald W, Hulsmeyer M. Crystal structure of human bone morphogenetic protein-2 at 2.7 A resolution. J Mol Biol 1999; 287:103-15.
66. Allendorph GP, Vale WW, Choe S. Structure of the ternary signaling complex of a TGFbeta superfamily member. Proc Natl Acad Sci USA 2006; 103:7643-8.
67. Breithaupt C, Schubart A, Zander H, Skerra A, Huber R, Linington C, Jacob U. Structural insights into the antigenicity of myelin oligodendrocyte glycoprotein. Proc Natl Acad Sci USA 2003; 100:9446-51.
68. Clements CS, Reid HH, Beddoe T, Tynan FE, Perugini MA, Johns TG, et al. The crystal structure of myelin oligodendrocyte glycoprotein, a key autoantigen in multiple sclerosis. Proc Natl Acad Sci USA 2003; 100:11059-64.
69. Rousseau F, Serrano L, Schymkowitz JW. How evolutionary pressure against protein aggregation shaped chaperone specificity. J Mol Biol 2006; 355:1037-47.
70. Coustou V, Deleu C, Saupe S, Begueret J. The protein product of the het-s heterokaryon incompatibility gene of the fungus *Podospora anserina* behaves as a prion analog. Proc Natl Acad Sci USA 1997; 94:9773-8.
71. Balguerie A, Dos Reis S, Ritter C, Chaignepain S, Coulary-Salin B, Forge V, et al. Domain organization and structure-function relationship of the HET-s prion protein of *Podospora anserina*. EMBO J 2003; 22:2071-81.
72. Curtis-Fisk J, Spencer RM, Weliky DP. Native conformation at specific residues in recombinant inclusion body protein in whole cells determined with solid-state NMR spectroscopy. J Am Chem Soc 2008; 130:12568-9.
73. Garcia-Fruitos E, Aris A, Villaverde A. Localization of functional polypeptides in bacterial inclusion bodies. Appl Environ Microbiol 2007; 73:289-94.
74. Curtis-Fisk J, Preston C, Zheng Z, Worden RM, Weliky DP. Solid-state NMR structural measurements on the membrane-associated influenza fusion protein ectodomain. J Am Chem Soc 2007; 129:11320-1.
75. Zhang H, Neal S, Wishart DS. RefDB: a database of uniformly referenced protein chemical shifts. J Biomol NMR 2003; 25:173-95.
76. Martinez-Alonso M, Gonzalez-Montalban N, Garcia-Fruitos E, Villaverde A. Learning about protein solubility from bacterial inclusion bodies. Microb Cell Fact 2009; 8:4.
77. Gonzalez-Montalban N, Garcia-Fruitos E, Villaverde A. Recombinant protein solubility—does more mean better? Nat Biotechnol 2007; 25:718-20.
78. Peternel S, Grdadolnik J, Gaberc-Porekar V, Komel R. Engineering inclusion bodies for non denaturing extraction of functional proteins. Microb Cell Fact 2008; 7:34.
79. Peternel S, Jevsevar S, Bele M, Gaberc-Porekar V, Menart V. New properties of inclusion bodies with implications for biotechnology. Biotechnol Appl Biochem 2008; 49:239-46.
80. Verel R, Tomka IT, Bertozzi C, Cadalbert R, Kammerer RA, Steinmetz MO, Meier BH. Polymorphism in an amyloid-like fibril-forming model peptide. Angew Chem Int Ed Engl 2008; 47:5842-5.
81. Petkova AT, Leapman RD, Guo Z, Yau WM, Mattson MP, Tycko R. Self-propagating, molecular-level polymorphism in Alzheimer's beta-amyloid fibrils. Science 2005; 307:262-5.
82. Deuerling E, Schulze-Specking A, Tomoyasu T, Mogk A, Bukau B. Trigger factor and DnaK cooperate in folding of newly synthesized proteins. Nature 1999; 400:693-6.